PROCESSES

Investigation into the influence of the interlayer temperature on machinability and microstructure of additively manufactured Ti-6Al-4V

Christina Fuchs[1] · Daniel Elitzer[2] · Heinz Werner Höppel[2] · Mathias Göken[2] · Michael F. Zaeh[1]

Abstract

The capability of wire and arc additive manufacturing (WAAM) to produce large, near-net-shaped parts with inexpensive equipment has led to the process being considered as one of the options to significantly decrease the buy-to-fly ratio in aircraft manufacture. Even so, there are several challenges associated with the process: achieving mechanical properties and microstructure similar to wrought material, as well as the low surface quality of the parts. The low surface quality is usually improved by milling. As with the microstructure, here too the question arises as to whether the process is comparable to milling wrought material. A significant factor influencing the microstructure according to literature is the interlayer temperature during the WAAM process. Therefore, the objective of this research was to study the influence of the interlayer temperature on the machinability and the microstructure of wire and arc additively manufactured Ti-6Al-4V. Consequently, the machinability was first determined for Ti-Al6-V4-parts manufactured with three different interlayer temperatures. Then, the macro- and microstructures were analyzed and, finally, the mechanical properties were determined. Contrary to expectations based on the state of the art, the machinability was not influenced by the interlayer temperature. This aligns with the mechanical properties and the macro- and microstructures, which are only slightly affected by the interlayer temperature.

Christina Fuchs and Daniel Elitzer have contributed equally to this work.

✉ Christina Fuchs
christina.fuchs@tum.de

Daniel Elitzer
daniel.elitzer@fau.de

Heinz Werner Höppel
hwe.hoeppel@fau.de

Mathias Göken
mathias.goeken@fau.de

Michael F. Zaeh
michael.zaeh@tum.de

[1] Institute for Machine Tools and Industrial Management, TUM School of Engineering and Design, Technical University of Munich, Boltzmannstrasse 15, Garching 85748, Germany

[2] Department of Materials Science and Engineering, Institute I: General Materials Properties, Friedrich-Alexander-Univer sität Erlangen-Nürnberg, Martensstrasse 5, Erlangen 91058, Germany

1 Introduction

Wire and arc additive manufacturing (WAAM) is considered to be an option to significantly decrease the buy-to-fly ratio in aircraft manufacture. This seems plausible since the process enables the additive manufacturing of large volume parts with inexpensive equipment [1]. With this buy-to-fly ratio, the mass of material needed to manufacture an aircraft component versus the mass of the material in the final component is quantified. In the conventional manufacturing process, parts are usually milled from slabs. In that case, the buy-to-fly ratio ranges up to 20 for the manufacture of Ti-6Al-4V (Ti-64) structural airplane components [2]. WAAM offers the option of significantly decreasing this ratio by manufacturing near-net-shaped components, which are thereafter milled to the final contour [1]. As the amount of removed material decreases by milling near-net-shaped components instead of slabs, so does the buy-to-fly ratio. This, in combination with Fronius' Cold Metal Transfer process (CMT), decreases the energy input and therefore

the penetration depth of the arc by mechanical deposition of the weld metal droplet via a pulsating wire electrode [3, 4].

However, there are some challenges associated with the process, such as the microstructure and mechanical properties. In order to be usable as an aircraft material, the mechanical properties of the wire and arc additively manufactured material (WAAM-material) must be comparable to those of the wrought material. In the case of the alloy Ti-6Al-4V, the typical wrought microstructure for aerospace applications comprises a globular and therefore isotropic microstructure consisting of coarse α-grains. These grains are surrounded by the β-phase. With this microstructure, yield strengths of 830 MPa and tensile strengths of at least 900 MPa in all directions should be achieved. Concerning Ti-6Al-4V WAAM-specimens typically show equiaxed primary β-grains near the baseplate, changing to an epitaxial grain growth and nucleation from existing grains at the fusion boundary with corresponding orientation [5, 6]. Within those primary β-grains, an acicular or a Widmannstätten structure forms depending on the cooling rate. Martina et al. found martensite in Ti 6Al-4V produced via Direct Energy Deposition (DED) after interpass rolling with 75 kN [7]. In higher areas of the additively manufactured part, the fraction of α-colonies increased because of the adaption of the cooling rate. Due to these microstructural changes throughout the specimen, several groups reported anisotropic mechanical behavior [8–11].

Since it is well known that the cooling rate is one of the decisive factors for the formation of the microstructure in titanium alloys, it plays a particular role and must be considered in additive manufacturing [12–14]. For the WAAM process, the cooling rate is adjustable by the temperature difference between the previous and the upcoming layer. The temperature down to which the previous layer is cooled is denoted as the interlayer temperature (ILT). Thus, this ILT becomes one of the crucial factors for the microstructural development in the part [15–17]. Due to the low thermal conductivity, a heat accumulation develops as the process progresses, which, unlike in the first layers, cannot be rapidly dissipated by conduction via the base plate [18]. Rodrigues et al. showed this heat accumulation for high strength low-alloy steels [19]. This leads to a unique and complex cooling history in time-controlled processes throughout the height of the component, resulting in different microstructures [20, 21].

Apart from the microstructure and mechanical properties, additional challenges associated with the WAAM process are the inferior surface quality, and the geometrical accuracy of the parts. Usually, these are improved by post-processing, for example by milling. The ease with which this machining process is performed is measured by the machinability of the

material [23]. Amongst other factors, it is dependent on the microstructure and the mechanical properties. Conventionally manufactured Ti-6Al-4V is considered to be a difficult-to-machine material compared to other materials, due to the low heat conductivity and low elasticity modulus [24]. This leads to high tool wear and thus to an expensive machining process. Indicators for the machinability are the cutting forces, the tool life and the surface roughness after machining [23]. Both cutting forces and surface roughness have already been used to determine the machinability of WAAM material, with varying results.

A significant difference between the machinability of wrought steel and WAAM steel (AISI H13) was shown by Montevecci et al. (2016) [25]. The authors measured higher cutting forces for the WAAM-material than for the wrought material. The measured hardness of the WAAM material was consistently higher as well. For a different steel (AISI 316 L) Masek et al. [26] conducted similar research with contrary results. While the average hardness of their WAAM-material was higher, the cutting forces were lower than for conventional material. The authors linked this to the microstructure of the components and local surface hardening on the wrought material. This influence of the microstructure on the machinability was also shown by Alonso et al. [27].

For Ti-6Al-4V, similar research was conducted by Veiga et al. [28]. The authors compared the cutting torque during up-milling and down-milling. They detected no statistically significant difference in the cutting torque between the two cutting strategies. Consistently, the mechanical properties of the material were detected to be independent of position and orientation in the sample. For a comparison with conventional material, Alonso et al. [29] presented a study on the machinability during drilling of WAAM Ti-6Al-4V. In comparison to conventional Ti-6Al-4V, a higher cutting torque and thrust force were detected for the WAAM-material. The authors concluded that the higher hardness and overall mechanical resistance of the material led to this behavior, even though their material had mechanical properties within the ASM specification.

Conclusively, the machinability of WAAM-material depends significantly on its microstructure and mechanical properties. Since the ILT has a strong influence on the microstructure and thus on the mechanical properties, the objective of this research was to study the influence of the ILT on the mechanical properties of as-built Ti-6Al-4V, and its machinability. Therefore, the machinability was first determined by evaluating the average process forces for cutting Ti-6Al-4V-parts manufactured with three different ILTs. Secondly, the macro- and microstructures were analyzed; and finally, the mechanical properties were determined.

2 Materials and methods

2.1 Wire and arc additive manufacturing

The samples were manufactured with the laboratory setup at the Institute for Machine Tools and Industrial Management (*iwb*) at the Technical University of Munich. This setup was comprised of a CMT Advanced 4000 R welding torch (Fronius International GmbH) mounted on a 6-axis industrial robot KR15/2 (Kuka AG). The welding was conducted in an enclosure with inert argon atmosphere, to prevent oxidation, with the oxygen level below 100 ppm. Ti-6Al-4V-plates with a thickness of 6 mm were used as the substrate material (base plate). The welding was executed in the CMT mode, with Ar4.8 as the welding torch gas, to keep the arc stable. The welding current was controlled by the CMT characteristic, the dynamic correction factor and the arc length correction factor. The samples were manufactured with a zigzag strategy as depicted in Fig. 1.

The width of the samples *w* was 24 mm, the length 80 mm, and they were built with 8 layers, resulting in a height of approximately 40 mm. The figure's z-axis is named the building direction, the figure's y-axis the welding direction. Two samples per ILT were manufactured. The ILT was determined with the setup proposed by Baier et al. [30]. Regions of interest (ROIs) were defined at the beginning of each layer. At these ROIs, a thermographic camera (X6900sc, FLIR Systems GmbH) was used to measure the ILT. After the deposition of a layer, the temperature was monitored in the ROI until the desired ILT was reached by cooling down from the melt. When the desired ILT was reached, the welding of the next layer was triggered. The welding parameters are listed in Table 1. Substrate heating was not used and the parts were not heat treated.

Table 1 The welding parameters for the manufacture of the WAAM-samples

Parameter	Value
Torch speed v_T	650 mm/min
Wire feed speed v_W	7 m/min
Interlayer temperature	200 – 350 – 500°C
Wire diameter	1.2 mm
Wavelength λ	4 mm
Offset o	6.1 mm
CMT characteristic	1085
Dynamic correction factor	3.7
Arc length correction factor	–14%
Number of deposited layers	8

2.2 Determination of the machinability

Before the determination of machinability, the surface waviness was removed from the samples at three sides by means of a roughing cut. Consequently, the machinability was determined during a cut with stationary engagement conditions, to enable the comparison with the conventional material. The cutting parameters and the engagement conditions for this cut are given in Table 2. Cutting was performed in a peripheral cut on a GROB 352T machining center (GROB-WERKE GmbH & Co. KG). Accordingly, the tool's feed direction was in the y-direction of the component, and the tool's normal direction in the x-direction (see Fig. 2). A dynamometer (Kistler 9257B, Kistler Instrumente GmbH) was used to measure the process forces at three feed rates. For the data acquisition, the Matlab Data Acquisition Toolbox (MathWorks) was used. The measurement frequency was 80 kHz, which was the maximum possible acquisition frequency.

To enable a comparison with the conventional material, three similar cuts were made in conventional Ti-6Al-4V.

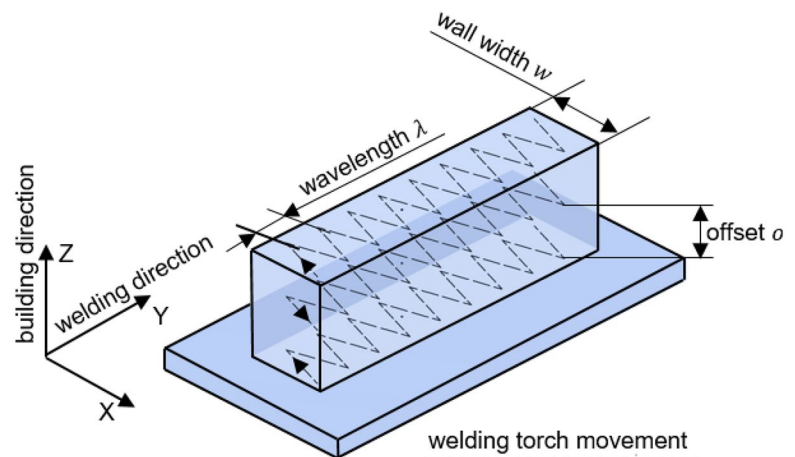**Fig. 1** The schematic of the manufacturing strategy for the WAAM-parts based on [22]

Table 2 The cutting parameters for the determination of the process forces

Parameter	Value
Feed rate per tooth f_z	0.04–0.06–0.08 mm/tooth
Spindle speed n	1100 U/min
Radial depth of cut	0.75 mm
Axial depth of cut	25 mm
Cutting strategy	Down milling
Tool diameter	16 mm
Number of teeth	4
Cutting material	Solide Carbide
Coating	TiAlN
Coolant strategy	Flood cooling

Here, the sampling frequency was 2.5 kHz, which was above any expected tooth engagement frequency. Setups for both the WAAM-material and the substrate material are depicted in Fig. 3.

2.3 Microscopy

The samples were analyzed at the Institute I: General Materials Properties (WW1) at the Friedrich-Alexander-Universität Erlangen-Nürnberg (FAU). All specimens were cut
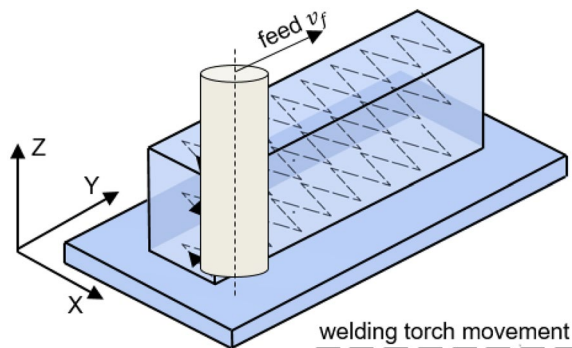
Fig. 2 The schematic of the milling strategy for the WAAM-parts
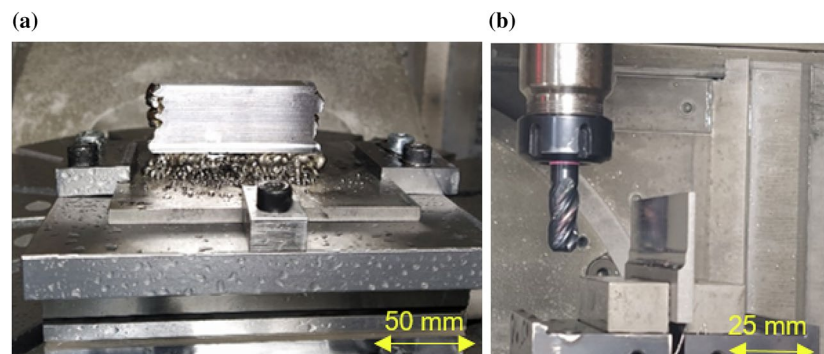
vertically, using corundum cut-off wheels, and examined with regard to their macro- and microstructures. The specimens were ground and polished using grinding paper and a 1 μm diamond suspension. In a final polishing step, the microstructure of the specimen was visualized using Kroll etchant and examined under a light microscope (Zeiss Axio) and a stereomicroscope (Wild Heerbrugg M420). Further samples were taken in both vertical and horizontal directions, so that any microstructural directional dependence could be investigated. These analyses were performed using a Zeiss CrossBeam 1540 EsB scanning electron microscope, combined with an Oxford INCA Energy 350 EDS system, in order to study chemical anomalies.

2.4 Mechanical testing

The quasi-static tests were performed with the laboratory setup of WW1 at FAU. Hardness measurements were conducted on a microscopic scale using a Vickers tip geometry on a Leco M 400-G with a load of 500 g and a holding time of 10 s. In each measured height a minimum of three indents were taken and analyzed according to DIN EN 6507 [31]. The flat tension specimens with a gauge length of 10 mm and a thickness of 1.75 mm were taken out of the middle of the additively manufactured samples in the welding direction. Tensile tests were performed at room temperature with a preforce of 250 N at a strain rate of 10^{-3} s^{-1} on an Instron 4505 equipped with a Hegewald & Peschke controlling system and a laser extensometer. Ten tensile test specimens were taken from each sample.

3 Results and discussion

3.1 Macro- and microstructure

To understand the milling behavior and its influence on the machinability, the macro- and microstructure must be carefully analyzed. Figure 4 shows a comparison of the macrostructures of specimens produced with different interlayer
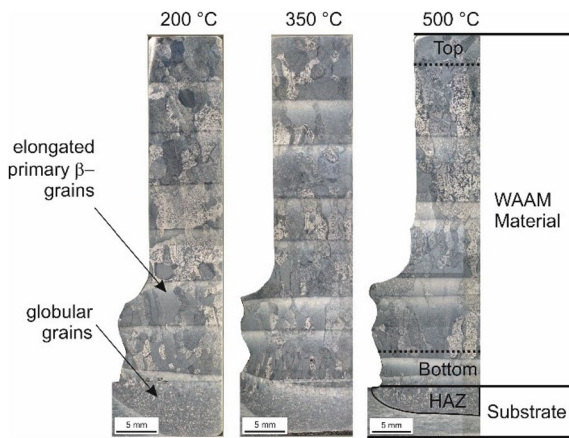
Fig. 3 The experimental setups to determine the process forces: **a** WAAM-material after the force measurement, **b** substrate material after the force measurement

Fig. 4 Comparison of the macrostructures achieved by changing the interlayer temperature, including a schematic representation of the top, bottom and HAZ measuring points for hardness measurement

temperatures. Typically, additively manufactured material consists of three main parts:

- the base plate made of the substrate material,
- the heat-affected zone (HAZ), and
- the welded part.

Every analyzed sample depicted in Fig. 4 revealed a globular microstructure at the substrate. The heat-affected zone within the substrate consists of a finer equiaxed microstructure, which forms lamellar α-phases within β-grains. This is similar to samples fabricated using constant interlayer time, see Elitzer et al. [32]. It can be seen that, with increasing ILT, the HAZ penetrates the base plate to a lesser extent. The first layers of the material processed at an ILT of 200°C are characterized by small, globular primary β-grains. This behaviour is also detectable for 350°C ILT; however, there is no evidence of this type of primary β-grains with an ILT at 500°C. As the

process continues, elongated grains are formed that grow beyond the weld boundaries. An increase in ILT leads to an enlargement in the grains. The latest layer of the specimen revealed more globular grains. The formation of primary β-grains has a direct influence on the resulting microstructure. Therefore, a comparison of the achieved microstructure depending on the height and the ILT is shown in Fig. 5.

Due to the high cooling rates of the first layers, a Widmannstätten structure was formed in the bottom area of the specimen. During the ongoing process, the recurring energy input led to a coarsening of lamellar microstructure. The temperature difference of the highest weld seam at the top of the specimen was still high enough for Widmannstätten structures to form. With increasing ILT, the temperature difference is reduced and, therefore, the cooling rate decreases. Consequently, noticeably more α-colonies were formed in the bottom of the part. Nevertheless, a Widmannstätten structure can still be identified. At 500°C ILT, the coarser α-colonial microstructure is visible, compared to the 350 and 200°C ILT throughout the additively manufactured part. The influence of this microstructural change on the mechanical properties was analyzed using hardness measurements and tensile tests.

3.2 Hardness measurement

Figure 6 compares the hardness and its standard deviation for different ILTs achieved in the building direction. The base plate shows a hardness of 321 ± 7 HV. Within the scatter, the hardness of the HAZ was found to be nearly constant for all ILTs at 321 ± 9 HV.

The hardness of the bottom part of the additively manufactured material at 200°C ILT is higher, compared to the base plate and the HAZ. Interestingly, the hardness decreases with increasing height from 328 ± 5 HV to 298 ± 9 HV. Due to the high temperature difference, a super saturated solid solution was formed. The reheating caused by the ongoing process led to a coarsening, which can be

Fig. 5 Comparison of microstructural images in building direction (BD) of the **a–c** bottom and **d–f** top part of the additively manufactured material
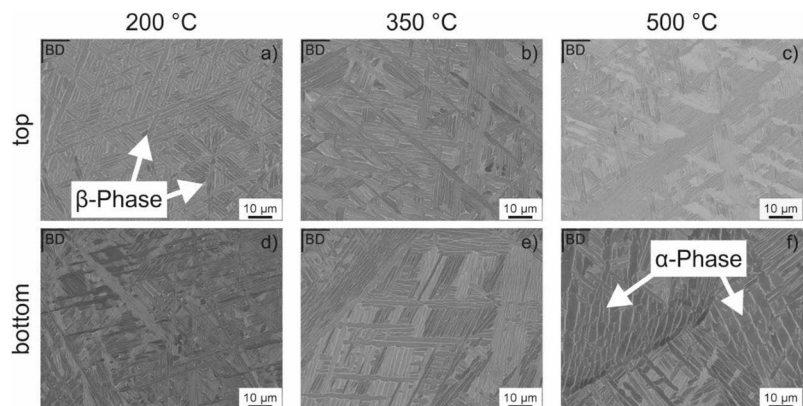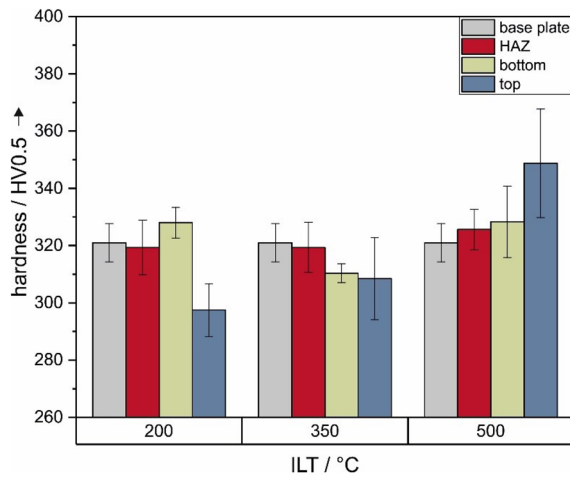
Fig. 6 Comparison of hardness measurements for the different ILTs depending on the height starting in the base plate

seen comparing the images taken at the bottom and top of the additively manufactured specimen in Figure 5. Due to this super saturation, precipitation processes can take place, which increases the hardness compared to the upper area. On the other hand, the saturation of alloying elements in case of incomplete diffusion in the titanium matrix leads to solid solution hardening.

An increase of the ILT to 350°C led to a decrease in the hardness in the lower areas, but to an increase in the top parts. A further increase in the ILT in turn increased the hardness to 328 ± 12 HV, and to 349 ± 19 HV for the higher areas. The change in the hardness distribution from 350°C to 500°C ILT is due to the influence of the interlayer temperature. At an ILT of 500°C, lower cooling rates were present which led to a higher α-phase fraction. This can be seen in Fig. 5. Due to the hexagonal crystal structure, the α-phase has a fundamentally higher hardness than the cubic β-phase. This, in combination with the higher α-phase fraction leads to an increased hardness in the specimen produced with an ILT of 500°C.

The analyzed data shows that in the higher areas of the specimens the scatter increases with increasing ILT. The change from a pure Widmannstätten structure towards an α-colony structure in Fig. 5a–c could be a reason for that increased scatter. Another reason for the increased scatter could be a more inhomogeneous cooling rate at higher ILTs in the most recent layer. Due to the thermal conductivity of titanium, this can lead to a laterally different microstructure, which is reflected in a larger scatter of the results at higher ILTs.

3.3 Tension tests

To evaluate the influence of the observed microstructural changes on the process forces during milling, tensile tests were performed, see Fig. 7. All tests were carried out in the welding direction and the results for yield strength Rp and tensile strength Rm, as well as the uniform elongation Ag and ultimate elongation A are averaged over the entire sample.

The yield strength at 200°C ILT was 804 ± 29 MPa with a tensile strength of 924 ± 26 MPa. An increase of the ILT to 350°C caused no change, neither in the yield strength (807 ± 23 MPa) nor in the tensile strength (921 ± 34 MPa). The same was found analyzing the uniform and ultimate elongation. The specimen produced at 500°C ILT has a slightly increased yield strength, at 822 ± 29 MPa, but within the scatter this difference can be neglected. The tensile strength of the specimen produced with an ILT of 500°C is 922 ± 34 MPa.

Tensile test data reveal that the ILT has a negligible influence on the overall strength of the specimens. A minor height dependency of the mechanical strength was detected. It was found that an ILT of 350 °C has the lowest and the specimen produced with an ILT of 200 °C the highest with a yield strength of 834 MPa $\pm$ 17 at the bottom and 799 MPa $\pm$ 11 at the top. It was also found that the strength in the middle of the tested samples was comparable to the top of the specimen. Since there was no evidence for porosity found the narrow scatter of the overall data roots from this minor height dependency. The yield strength shows a slight increase but stays within the scatter, whereas the tensile strength is constant over all tested parameters. The uniform elongation and the elongation at fracture are also constant within the margin of scatter.
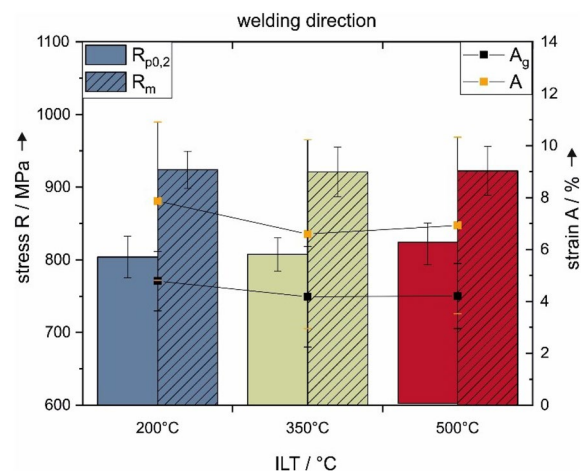

Fig. 7 Overview of the tension test results in welding direction

3.4 Machinability

For each cut, the forces in the dynamometer's x, y, and z-direction were obtained. The x-direction corresponds to the tool's normal direction, the y-direction to the tool's feed direction and the z-axis to the tool's axial direction. Figure 8 depicts the measured force signal in the y-direction for an exemplary cut.

Next, the signals were filtered with a moving average filter with a duration of four spindle rotations. Then, the area of interest for each feed rate was determined. An interval of at least 0.8 s was disregarded at the change between feed rates, to allow for stable cutting conditions within the duration of the measurement (see Fig. 9).

For each interval of the feed rate, the mean force as well as the standard deviation of the unfiltered signal were determined. The standard deviation of the unfiltered signal gives a scale of the process forces' inherent fluctuations due to the kinematics of the milling process. In Table 3, the mean forces and their standard deviations are listed for all ILTs and the substrate material. In Fig. 10, the results for the different ILTs, with two samples per temperature, in comparison to the substrate material, with three samples, are depicted.

During the peripheral milling process the main cutting is performed along the tool helix [33]. Therefore, due to the cutting parameters, the forces in the axial direction are much lower, and are not depicted in Fig. 10, but are instead listed in the appendix A. The mean forces in the tool's normal direction range from 263.18 ± 82.62 N to 414.82 ± 94.47 N. For the feed direction, the mean forces range from 134.82 ± 40.28 N to 246.69 ± 96.47 N.
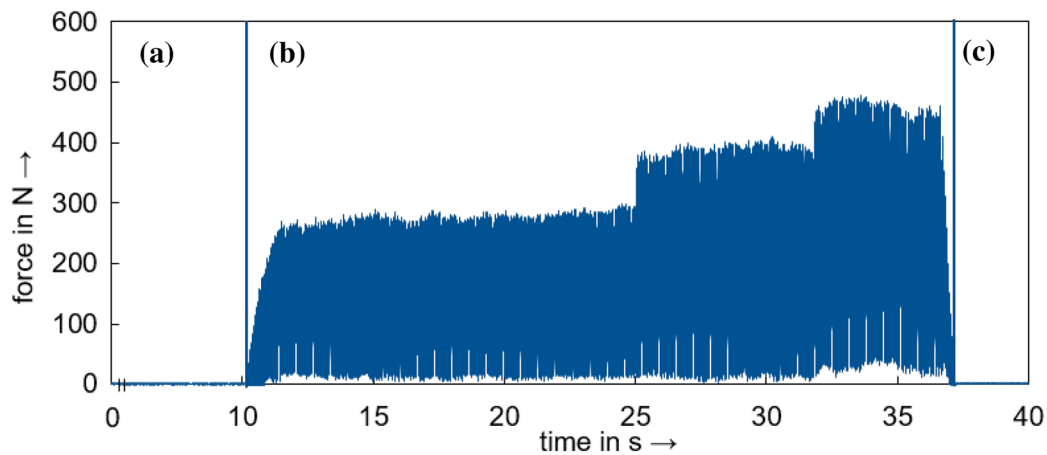

Fig. 8 Exemplary depiction of the measured forces: **a** start of the measurement without cutting, **b** cutting, **c** end of the measurement without cutting
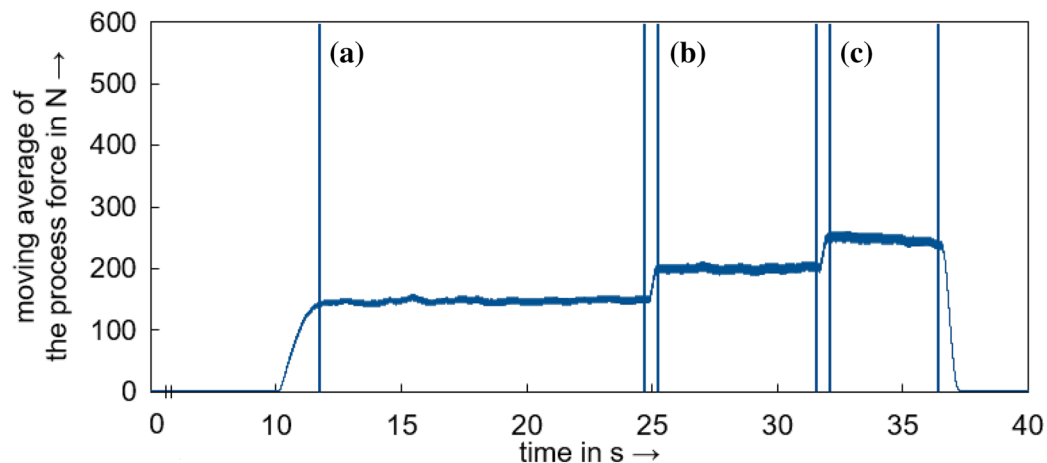

Fig. 9 Exemplary depiction of a filtered force signal in the y-direction: **a** feed rate 0.04 mm/tooth, **b** feed rate 0.06 mm/tooth, **c** feed rate 0.08 mm/tooth
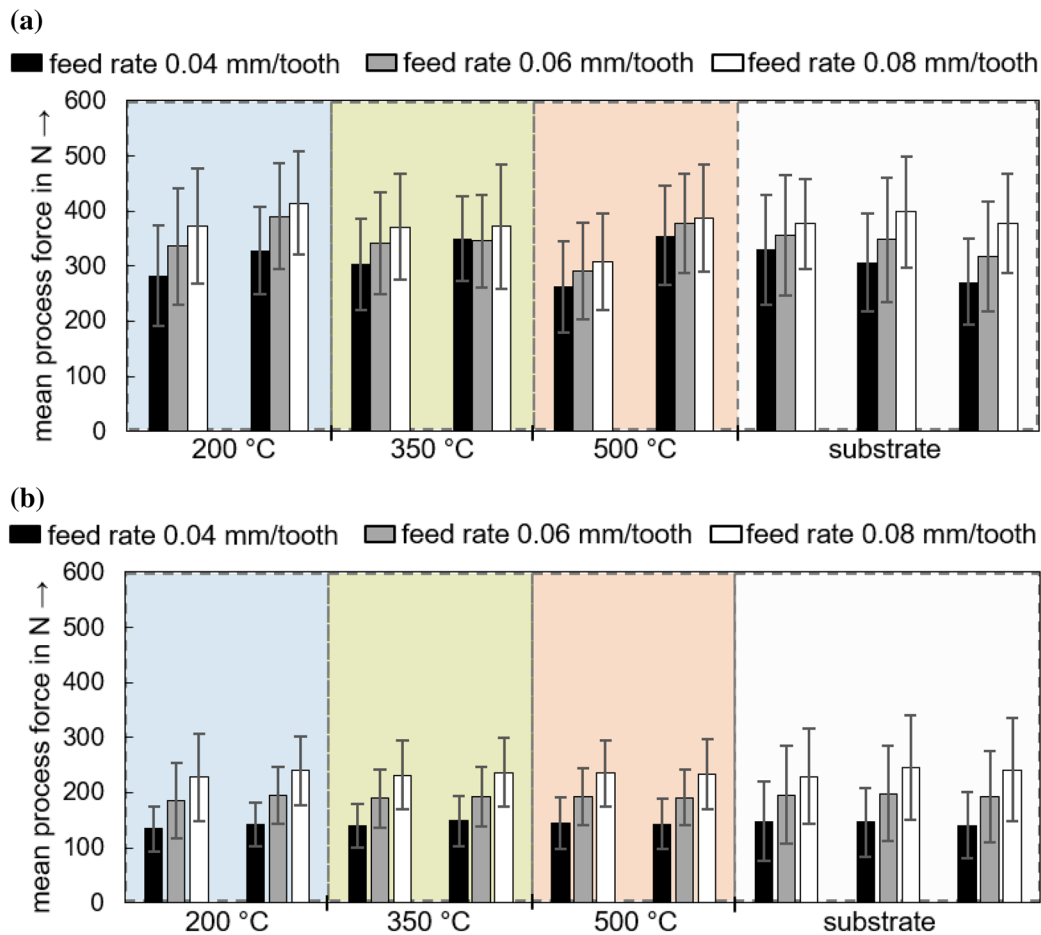
(a)

(b)

Fig. 10 The absolute mean process force in **a** the tool's normal direction and **b** the tool's feed direction for the different feed rates and interlayer temperatures

Firstly, as could be expected from literature, for each sample, the mean process force increases with the rising feed rate [23]. Secondly, the process forces in the tool's normal direction are higher than along the feed direction. This holds true both for the WAAM-material and the substrate material. The behavior is therefore likely linked to the setup, the material's machinability and the cutting parameters in an analogous way. Thirdly, there is no influence of the different interlayer temperatures on the process forces in the welding direction. Finally, no significant difference was detected between the substrate material and the WAAM-material, independent of the ILT.

4 Discussion

Despite the use of constant ILTs instead of constant interlayer-time, which led to the accumulation of energy in the ongoing process and thus to different cooling rates within a sample, it was found that despite a constant ILT (e.g. 200°C applied throughout the sample), a height-dependent microstructure emerges. This is due to the cold substrate plate and the system's saturation with thermal energy as the number of layers increases. Therefore, the cooling rate declines. In addition, the constant supply of additional thermal energy leads to a coarsening in the lower region of the additively manufactured wall. This is noticeable in the local hardness measurement. At lower ILTs, a super-saturated solid solution forms in the first layers, from which precipitates can form over the further course of the process. This may be the reason for an increased hardness despite a coarsened microstructure in the lower areas of the additively manufactured specimen. Increasing the ILT to 350 °C reduces the temperature difference between the weld to be applied and the weld pool, resulting in a lower cooling rate. As a result, the supersaturation just mentioned decreases and the effect of solid solution hardening diminishes. Due to the increased ILT, α-colonies can now also be identified in the lower areas.

It can be concluded that cooling rates comparable to those of upper layers have already been achieved within the first layers. Since this differs from specimen produced with lower ILTs, this results in more comparable mechanical properties of the specimen throughout the height, compared to an ILT of 200 °C, see Fig. 6.

However, this dependence was not identified in tensile tests since the overall strength of each specimen was comparable. Presumably, this may be because the hardness measurement has a local resolution, and therefore plays a negligible role in tensile tests. Nonetheless, these results contradict those of other research groups that have measured ILT-dependent strength [15, 34]. These contradictions may be due to the lower number of layers used in this study, and can be traced back to the different thermal household of the different specimens. Since the grain boundary density is higher in the welding direction compared to the building direction, a directional dependency can be expected. Because of the sample height, however, this could not be investigated and would have had a negligible influence on the machinability due to the milling setup. Concerning the machinability of the material, the influence of the ILT on the mean process forces is negligible, resulting in a comparable machinability. Reasons for this are the comparable yield strength and the hardness of the components. Due to the milling strategy, the height-dependent hardness in the building direction does not influence the resulting process forces. It is likely that, for a different milling strategy—either parallel to the building direction or cutting individual layers singularly, for example during micromilling—the process forces would most likely exhibit a dependency on the component height. At the same time, the measured hardness of the base plate is within the standard deviation of the hardness on the bottom and top of the WAAM-material. This supports the result that there is no discernable difference in the process forces for the machining of the WAAM-material in comparison to the substrate material.

5 Conclusion

The objective of this research was to study the influence of the ILT on the machinability and the microstructure of WAAM-manufactured components. For this purpose, samples with three different ILTs were manufactured and their machinability in peripheral milling was determined. Additionally, the macro- and microstructure as well as the hardness and the yield strength were determined. The key findings are:

- Despite a constant ILT, a height-dependent microstructure develops, especially at lower ILTs.
- At a higher ILT, a coarsened, colony-like microstructure is established near the substrate plate.
- No influence of the ILT on the machinability in the welding direction of the WAAM-material was detected.
- A machinability of the wire and arc additively manufactured Ti-6Al-4V comparable to the machinability of the substrate material is achievable.

These findings are in contrast to the previous state of the art, which indicates a connection between the mechanical properties and the ILT. A reason for the results of this research might be the size of the WAAM-samples. Due to the lower heat accumulation in smaller samples, the heat can dissipate more easily into lower areas. Consequently, a different microstructure is achieved because of the higher cooling rates in smaller samples compared to bigger ones. The cooling rates of the analyzed specimens might have been too close to each other for a major influence on mechanical properties and machinability to show up. Therefore, the specimen volume, more precisely the thermal household, was found to have a significant influence on the microstructure and the resulting mechanical properties.

In the future, research should be performed on this subject, especially to determine if the size of the parts does indeed influence the connection between the ILT and the microstructure. This would impact the economics of the process chain, since for larger structures a lower ILT might be necessary, while, for smaller parts, a higher ILT and thus a shorter idle time might be feasible. Then, appropriate values for the ILT should be determined, in order to achieve the best microstructure for the chosen application. Finally, a thermal model of the correlation between ILT and microstructure should be established. The thermal model should include the detailed heat transfer into the substrate and between the deposited layers. This would enable an indepth study of the cooling rate profile and enable the simulation and the prediction of the resulting microstructure and improve the applicability of the process chain.

Due to the chosen setup, the influence of the microstructural changes in the building direction on the machinability could not be determined. For more complex parts, it is expected that milling processes are necessary which would be influenced by these changes. Therefore, studies should be performed to analyse this influence.

Appendix A Process forces

See Table 3 in the appendix.

Table 3 The mean process forces in N with standard deviations

ILT	feed rate in mm/tooth	force in X-direction: tool's radial direction in N		
		sample 1	sample 2	sample 3
200 °C	0.04	282.33 ± 90.90	329.35 ± 79.07	
	0.06	336.22 ± 106.04	390.83 ± 95.11	
	0.08	373.69 ± 104.75	414.82 ± 94.47	
350 °C	0.04	303.51 ± 82.16	350.19 ± 77.01	
	0.06	341.92 ± 92.77	346.02 ± 83.75	
	0.08	371.34 ± 95.43	371.95 ± 112.38	
500 °C	0.04	263.18 ± 82.62	355.87 ± 90.00	
	0.06	291.88 ± 88.35	378.13 ± 89.22	
	0.08	308.20 ± 87.01	387.76 ± 96.42	
substrate	0.04	330.11 ± 99.82	307.84 ± 89.19	271.68 ± 77.60
	0.06	355.46 ± 109.41	348.15 ± 113.25	317.47 ± 99.93
	0.08	377.29 ± 81.96	398.52 ± 99.98	377.34 ± 89.75

ILT	feed rate in mm/tooth	force in Y-direction: tool's feed direction in N		
		sample 1	sample 2	sample 3
200 °C	0.04	134.82 ± 40.28	142.12 ± 38.88	
	0.06	185.84 ± 67.56	196.07 ± 51.18	
	0.08	227.94 ± 79.02	239.98 ± 63.22	
350 °C	0.04	139.73 ± 39.91	148.69 ± 44.66	
	0.06	189.64 ± 52.75	193.25 ± 54.02	
	0.08	232.05 ± 62.08	237.07 ± 63.03	
500 °C	0.04	143.96 ± 46.95	143.67 ± 45.66	
	0.06	192.29 ± 51.69	191.21 ± 50.39	
	0.08	235.45 ± 60.58	234.19 ± 63.32	
substrate	0.04	148.36 ± 72.14	146.36 ± 62.23	141.17 ± 59.97
	0.06	196.20 ± 89.52	198.84 ± 87.46	192.89 ± 82.46
	0.08	230.14 ± 87.00	246.00 ± 95.17	242.16 ± 92.78

Table 3 (continued)

ILT	feed rate in mm/tooth	force in Z-direction: tool's axial direction in N		
		sample 1	sample 2	sample 3
200 °C	0.04	63.12 ± 30.67	62.10 ± 21.81	
	0.06	87.73 ± 34.39	88.25 ± 29.00	
	0.08	113.20 ± 40.83	114.45 ± 34.74	
350 °C	0.04	62.97 ± 25.45	62.86 ± 23.68	
	0.06	89.02 ± 33.47	90.10 ± 30.44	
	0.08	114.31 ± 39.76	112.55 ± 35.50	
500 °C	0.04	65.37 ± 21.92	64.79 ± 25.07	
	0.06	94.04 ± 27.89	92.76 ± 27.22	
	0.08	120.92 ± 36.01	117.50 ± 33.31	
substrate	0.04	46.43 ± 34.78	54.91 ± 29.37	55.03 ± 28.65
	0.06	67.01 ± 43.69	75.43 ± 41.95	77.43 ± 40.56
	0.08	81.18 ± 42.69	98.35 ± 47.56	100.46 ± 46.34

Declarations

Conflict of interest The authors declare that they have no conflict of interest. The funders had no role in the design of the study; in the collection, analyses, or interpretation of data; in the writing of the manuscript, or in the decision to publish the results.

References

1. Martina F, Williams S (2015) Wire+arc Additive Manufacturing vs. A Cost Comparison, Traditional Machining from Solid
2. Allen J (2006) An Investigation into the Comparative Costs of Additive Manufacture vs. Machine from Solid for Aero Engine Parts
3. Selvi S, Vishvaksenan A, Rajasekar E (2018) Cold metal transfer (CMT) technology - An overview. Defence Technology 14:28–44
4. Pickin CG, Young K (2013) Evaluation of cold metal transfer (CMT) process for welding aluminium alloy. Sci Technol Weld Joining 11:583–585
5. Kurz W, Bezençon C, Gäumann M (2001) Columnar to equiaxed transition in solidification processing. Sci Technol Adv Mater 2:185–191
6. Gäumann M, Bezençon C, Canalis P, Kurz W (2001) Single-crystal laser deposition of superalloys. Acta Mater 49:1051–1062
7. Martina F, Colegrove PA, Williams SW, Meyer J (2015) Microstructure of interpass rolled wire + arc additive manufacturing Ti-6Al-4V components. Metall Mater Trans A 46:6103–6118
8. Wang F, Williams S, Colegrove P, Antonysamy AA (2013) Microstructure and mechanical properties of wire and arc additive manufactured Ti-6Al-4V. Metall and Mater Trans A 44:968–977
9. Vilaro T, Colin C, Bartout JD (2011) As-Fabricated and Heat-Treated Microstructures of the Ti-6Al-4V Alloy Processed by Selective Laser Melting. Metall Mater Trans A 42:3190–3199
10. Edwards P, O'Conner A, Ramulu M (2013) Electron Beam Additive Manufacturing of Titanium Components. J Manuf Sci Eng 135:525
11. Amsterdam E, Kool GA (2009) High Cycle Fatigue of Laser Beam Deposited Ti-6Al-4V and Inconel 718. ICAF 2009, Bridging the Gap between Theory and Operational Practice
12. Lütjering G (1998) Influence of processing on microstructure and mechanical properties of $(\alpha + \beta)$ titanium alloys. Mater Sci Eng, A 243:32–45

13. Pederson R (2002) Microstructure and Phase Transformation of Ti-6Al-4V

14. Ahmed T, Rack HJ (1998) Phase transformations during cooling in $\alpha + \beta$ titanium alloys. Mater Sci Eng, A 243:206–211

15. Ma Y, Cuiuri D, Shen C, Li H, Pan Z (2015) Effect of interpass temperature on in-situ alloying and additive manufacturing of titanium aluminides using gas tungsten arc welding. Addit Manuf 8:71–77

16. Geng H, Li J, Xiong J, Lin X (2016) Optimisation of interpass temperature and heat input for wire and arc additive manufacturing 5A06 aluminium alloy. Sci Technol Weld Joining 22:472–483

17. Yang D, Wang G, Zhang G (2017) Thermal analysis for single-pass multi-layer GMAW based additive manufacturing using infrared thermography. J Mater Process Technol 244:215–224

18. Zhao H, Zhang G, Yin Z, Wu L (2011) A 3D dynamic analysis of thermal behavior during single-pass multi-layer weld-based rapid prototyping. J Mater Process Technol 211:488–495

19. Rodrigues TA et al (2019) Wire and arc additive manufacturing of HSLA steel. Addit Manuf 27:440–450

20. Kobryn PA, Semiatin SL (2001) The laser additive manufacture of Ti-6Al-4V. JOM 53:40–42

21. Kobryn P, Semiatin S (2003) Microstructure and texture evolution during solidification processing of Ti-6Al-4V. J Mater Process Technol 135:330–339

22. Fuchs C, Baier D, Semm T, Zaeh MF (2020) Determining the machining allowance for WAAM parts. Prod Eng Res Devel 14:629–637

23. Huda Z (2021) Machining processes and machines. First edition edn, CRC Press

24. Davim JP (2014) Machining of titanium alloys. Materials forming, machining and tribology. Springer, New York

25. Montevecchi F et al (2016) Cutting Forces Analysis in Additive Manufactured AISI H13 Alloy. Procedia CIRP 46:476–479

26. Masek P et al (2019) MACHINABILITY THE AISI 316 STAINLESS STEEL AFTER PROCESSING BY VARIOUS METHODS OF 3D PRINTING. MM Science Journal 2019:3338–3346

27. Alonso U, Veiga F, Suárez A, Gil Del Val A (2021) Characterization of Inconel 718®superalloy fabricated by wire Arc Additive Manufacturing. *Journal of Materials Research and Technology***14**, 2665–2676 (2021)

28. Veiga F, Gil Del Val A, Suárez A, Alonso U (2020) Analysis of the Machining Process of Titanium Ti6Al-4V Parts Manufactured by Wire Arc Additive Manufacturing (WAAM). Materials (Basel, Switzerland) **13**

29. Alonso U, Veiga F, Suárez A, Artaza T (2020) Experimental Investigation of the Influence of Wire Arc Additive Manufacturing on the Machinability of Titanium Parts. Metals 10:24

30. Baier D, Wolf F, Weckenmann T, Lehmann M, Zaeh MF (2022) Thermal process monitoring and control for a near-net-shape Wire and Arc Additive Manufacturing. Prod Eng Res Devel 16:811–822

31. DIN EN 6507 – Metallische Werkstoffe – Härteprüfung nach Vickers [eng.: Metallic materials - Vickers hardness test]

32. Elitzer D et al (2023) Development of Microstructure and Mechanical Properties of TiAl6V4 Processed by Wire and Arc Additive Manufacturing. Adv Eng Mater 25:2201025

33. Altintas Y (2012) Manufacturing automation. 2 edn, Cambridge University Press, Cambridge

34. Derekar K et al (2019) Influence of Interpass Temperature on Wire Arc Additive Manufacturing (WAAM) of Aluminium Alloy Components. MATEC Web of Conferences 269:05001